On Melting of Electrodes during Electro-Slag Remelting

Abdellah KHARICHA,[1]* Andreas LUDWIG[2] and Menghuai WU[1]

1) Christian Doppler Lab for Advanced Simulation of Solidification and Melting, Dept. of Metallurgy, Montanuniversitaet Leoben, Franz-Joseph Strasse 18, 8700 Leoben, Austria.
2) Dept. of Metallurgy, Montanuniversitaet Leoben, Franz-Joseph Strasse 18, 8700 Leoben, Austria.

In this paper a numerical investigations on the thermal state and on the tip shape of a melting electrode during electro-slag remelting are presented. In the first part the heat necessary to melt an electrode with a flat tip shape is calculated. It is shown that to keep a constant melting rate, the heat supplied to the electrode must be continuously changed. The results for different electrode descend rates, corresponding to different melting rates, are presented. In the second part the melting process was simulated with the help of a numerical model which takes into account simultaneous action of magneto-hydrodynamics, and thermal and phase changes phenomena. The model assumes no mould current. Simulations were performed with constant applied current and electrode descend velocity. The simulations have shown that the coupling between the melting rate and the Joule heat release process is very unstable. One result showing a stable electrode tip is presented and discussed in details.

KEY WORDS: electro-slag remelting; melting; magneto-hydrodynamic; Joule heating; droplets; heat transfer; electrode shape; Stefan problem.

1. Introduction

In the past few years, remelting technologies have played an important role in producing special materials and the number of Electro-Slag Remelting (ESR) units is continuously growing. In the ESR process an as-cast electrode is immersed into a hot slag such that droplets depart from the melting electrode, pass through the turbulently flowing slag and finally feed a liquid metal pool which then solidify directionally. Hereby, the heat provided by the slag to the electrode determines the efficiency of the melting process. An analysis of the heat balance of the ESR process has indicated that typically 25% of the heat generated is transferred to the electrode.[1] Electrochemical reactions at the electrode surface can also contribute to the heat provided to the electrode. Significantly higher melt-rates are observed for cathodic electrodes (DC ESR) melting in air than in argon.[2] This phenomenon is neither observed for DC anodic electrodes nor for 60 Hz AC electrodes. For these reasons, the origin of difference in melting efficiency of different power sources was attributed to some electrochemical modification in composition of the slag, or to the additional generation of heat due to the formation of an over-potential at the electrode interface. Jardy et al.[3] have shown that the hydrodynamic is also an important factor controlling the heat transfer to the electrode. The highest heat transfer rate was predicted for the case where the buoyancy forces dominate the electromagnetic forces. The development of turbulence just under the electrode is also related to the formation and departure

of the droplets.[4,5] The deviation of electromagnetic fields by the liquid metal faucets generates strong turbulences that surely impact on the melting rate.

Despite of its importance, few works focus on the thermal state of the electrode.[6,7] Mitchell et al.[6] described some experiments where the electrode temperature was measured at a laboratory scale ESR furnace. Additionally, a complex steady-state two dimensional (2D) model of the heat balance was suggested. The model provided fairly good results when compared with the experimental temperature profiles. A simpler analytical model was proposed by Mendrowsky et al.[7] in which both conduction and radiation from the slag surface were taken into account. Based on this model the temperature ranges were found in good agreements with experimental data provided in Mitchell et al.[6] The computed results also suggested that thermal radiation is unlikely to be important in comparison with the heat conduction. Tacke et al.[8] used a numerical model to analyse the relation between the temperature field and the melting profile of the electrode. This model was able to compute both temperature and melting profile simultaneously using a False Position algorithm. Several experiments with different electrode descend rates were performed, where the slag temperature was measured and the electrode tip shape was investigated. To fit the experimental results, their computation needed an empirical slag/electrode heat transfer coefficient, which was found to vary between 2 000 and 4 500 W/m²K from one experiment to another.

All these models imposed room temperature at a certain distance from the electrode tip, which means that the heat diffusion has not the time to reach the other extremity of the electrode. However, the electrode is a finite and closed sys-

tem, which is strongly heated during the whole remelting time. The issue of the electrode melting is clearly a Stefan problem where both the temperature field and the melting front velocity are unknown. Assuming that the electrode is semi-infinite, Zien[9] suggested an approximate analytical solution of this ablation problem with the help of the approximate integral method. This method was suggested to be used in the control system for the melting of electrodes in the vacuum arc remelting (VAR) process.[10]

In the present investigation this one dimensional (1D) Stefan problem is solved numerically. First the time dependant heat necessary to melt an electrode with a desired constant melting rate is calculated. For that a 1D thermal analysis is performed on an electrode which is ablated according to quantity of heat received from the slag. Then a 2D simulation including the slag media is performed. The influence of the electromagnetic field as well as the hydrodynamic is considered.

2. One Dimensional Model Description for Energy Balance Analysis of Electrode

In order to solve the energy equation in a moving boundary domain, we consider the case shown in **Fig. 1**. At the time t, the electrode has a length of $s(t)$ and moves downwards towards the slag at a speed u_e. The electrode tip (bottom) is assumed to melt uniformly to form a flat interface. The melting temperature of the electrode, $T_{interface}$, is assumed to be equal to the liquidus temperature of the electrode material T_L. The origin of the coordinate system is fixed at the top extremity of the electrode. If the solid electrode melts uniformly at the level of the slag surface, the coordinate system moves with the electrode at the specified speed $u_e = -ds/dt$. The heat transfers at the top and lateral boundaries as well as the heat generated by Joule heat dissipation are neglected. Thus, we have solved the following one dimensional (1D) heat transport problem

$$\frac{\partial\left(\rho C_p T\right)}{\partial t} = \frac{\partial}{\partial x}\left(k\frac{\partial T}{\partial x}\right) \quad \text{for } t > 0 \text{ and } 0 < x < s(t), \cdots (1)$$
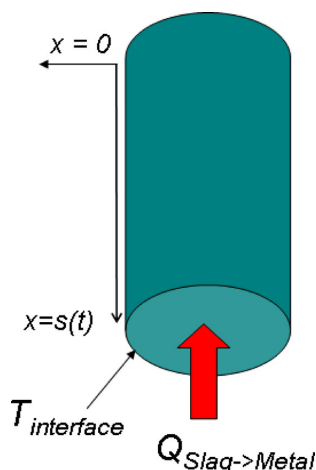
with the following boundary conditions

Fig. 1. Coordinate set up for the electrode. (Online version in color.)

$$\left.\frac{\partial T}{\partial x}\right|_{x=0} = 0 \quad \text{and} \quad \left.T\right|_{x=s(t)} = T_{interface} \quad \text{for } t \geq 0, \ \ \cdots (2a)$$

$$k\left.\frac{\partial T}{\partial x}\right|_{x=s(t)} - \rho\Delta H\frac{ds}{dt} = Q_{Slag\rightarrow Metal}, \quad \text{for } t \geq 0. \ \cdots (2b)$$

Here, ρ is the density, C_p the heat capacity, T the temperature, t the time, k the thermal conductivity, ΔH the latent heat of fusion and $Q_{Slag\rightarrow metal}$ is the heat that must be provided from the slag to the electrode to achieve the given melting rate.

Usually, the Stefan problem consists in predicting the velocity of the melting front for a given or computed heat flux. In the present problem the unknown quantity is the heat flux $Q_{Slag\rightarrow metal}$ rather than the melting rate. Since the melting rate which is given by electrode descent speed, u_e, is set to be constant, the latent heat of fusion is also constant. The real unknown quantity of the problem is the heat diffusing into the electrode, $q = -k\left.\frac{\partial T}{\partial x}\right|_{x=s(t)}$, which depends on how much the electrode is heated during the remelting process. Thus, q is time and u_e dependant, its magnitude varies from the moment when the electrode touch the slag to the moment when the last layer of the electrode disappears.

The moving boundary-value problem governed by Eqs. (1) and (2) can be transformed into a fixed one by means of the mapping $(t, x) \rightarrow (\tau, \zeta)$,where $\tau = t$ and $\zeta = x/s(t)$, so that the problem becomes

$$\frac{\partial}{\partial\tau}(sT) = \frac{\partial}{\partial\zeta}\left(\frac{k}{\rho C_p}\frac{1}{s}\frac{\partial T}{\partial\zeta}\right) + \xi\frac{\partial}{\partial\zeta}\left(\frac{ds}{d\tau}T\right) \quad \cdots (3)$$

for $\tau > 0$ and $0 < \zeta < 1$,

with boundary conditions

$$\left.\frac{\partial T}{\partial\zeta}\right|_{\zeta=0} = 0, \quad \left.T(\tau)\right|_{\zeta=1} = T_{interface}, \quad \text{for } \tau \geq 0 \ \cdots (4a)$$

$$\frac{k}{s}\left.\frac{\partial T}{\partial\zeta}\right|_{\zeta=1} - \rho\Delta H\frac{ds}{d\tau} = Q_{Slag\rightarrow Metal}, \quad \text{for } \tau \geq 0 \ \cdots (4b)$$

The system of equations, Eqs. (3) and (4), are solved with the properties given in **Table 1** for steel.

3. Two Dimensional Model Description for ESR Process Simulation

In a real system the heat flux to the electrode depends on the slag temperature and on the energy transport phenomena. Due to the good mixing condition occurring within the slag, its temperature distribution can be assumed uniform. However, the effective slag/electrode heat transfer coefficient controlled by the turbulent velocity field might not be uniform over entire electrode/slag surface. The electrode can then melt non-uniformly. Depending on the electrode descend velocity, it can be difficult to develop a flat or a stable electrode shape. In order to explore the complex coupling which exists between the imposed electric current, the melting rate and the thermal condition of the electrode, it is necessary to build a model in which all mechanisms are coupled. The present study uses a 2D axis-symmetrical magne-

Table 1. Averaged material properties used.

Slag

Density ρ	2 700 kg/m^3
Viscosity μ	0.0025 kg/m/s
Specific heat, liquid C_p	1 200 J/kg/K
Thermal expan. Coefficient β	2.5×10^{-4} K^{-1}
Electric conductivity, σ 1 000 K	1.0×10^1 (Ωm)$^{-1}$
Electric conductivity, σ 1 870 K	1.2×10^2 (Ωm)$^{-1}$
Thermal conductivity, k 2 000 K	3.24 W/m/K
Thermal conductivity, k 750 K	0.41 W/m/K
Liquidus T_L	1 650 K
Fictitious solidus T_S	1 625 K

Steel

Density ρ	6 850 kg/m^3
Viscosity μ	0.006 kg/m/s
Specific heat, liquid C_p	750 J/kg/K
Latent heat of fusion ΔH	2.7×10^5 W/kg
Thermal expan. Coefficient β	1×10^{-4} K^{-1}
Electric conductivity σ	7.0×10^5 (Ωm)$^{-1}$
Thermal conductivity k	26 W/m/K
Liquidus T_L	1 750 K
Fictitious solidus T_S	1 725 K

Air

Density ρ	1.5 kg/m^3
Effective viscosity μ	1e-2 kg/m/s
Specific heat C_p	1 000 J/kg/K
Effective thermal conductivity k	2 W/m/K

Interfacial tension

Metal/slag	1 N/m
Metal/air	1.3 N/m
Slag/air	0.5 N/m

Table 2. Mathematical expression of the hydrodynamic, thermal and electric boundary conditions.

Top electrode boundary (Inlet boundary)

$$U_z = -u_e, \ U_r = 0$$

$$T = 300 \ K, \ -\sigma \frac{\partial \phi}{\partial z} = \pm \frac{l_0}{\pi R_e^2} \ (5 \ \text{Hz})$$

$$\frac{\partial A_z}{\partial z} = 0, \frac{\partial A_r}{\partial z} = 0$$

Top air boundary (Pressure inlet)

$$P = 0, T = 300 \ K, -\sigma \frac{\partial \phi}{\partial z} = 0, \frac{\partial A_z}{\partial z} = 0, \frac{\partial A_r}{\partial z} = 0$$

Mould (wall)

$$U_z = -\frac{R_e^2}{R_m^2} u_e, \ U_r = 0, \frac{\partial \phi}{\partial r} = 0$$

Mould/Air: $\varepsilon_r = 0.8$, $H = 50$ W/(Km^2), $T_e = 400$ K

Mould/Slag: $T_e = 1\,650$ K

Mould/Metal (contact): $\varepsilon_r = 0.1$, $H = 1\,500$ W/(Km^2), $T_e = 450$ K

Mould/Metal (No contact): $\varepsilon_r = 0.8$, $H = 20$ W/(Km^2), $T_e = 400$ K

$$\frac{\partial A_z}{\partial r} = \frac{l_0}{2\pi R_m}, \ A_r = 0$$

Bottom (outlet boundary)

$$U_z = -\frac{R_e^2}{R_m^2} u_e, \ U_r = 0, \phi = 0, \frac{\partial A_z}{\partial z} = 0, \frac{\partial A_r}{\partial z} = 0$$

Table 2.

3.1. Electromagnetic Field

The electromagnetic field is solved by using the electric field ϕ and the magnetic potential vector $\vec{A}$. The electric potential equation is extracted from the equation of the conservation of the electric current $\vec{j}$:

$$\nabla \cdot \vec{j} = 0 \quad \text{with} \quad \vec{j} = -\sigma \frac{\partial \vec{A}}{\partial t} - \sigma \nabla \phi \ \dots \dots (5)$$

A time varying electric current flow is applied at the top boundary of the cooper mould. The mould is in electric contact with the baseplate. The electric current is not allowed to cross the solid slag skin.[13,14] A constant electric potential ($\phi = 0$) is applied at the top boundary of the solid electrode. The magnetic field $\vec{B}$ is extracted by solving the magnetic potential vector $\vec{A}$ equation:

$$\nabla \times \left(\frac{1}{\mu_0} \nabla \times \vec{A} \right) - \nabla \left(\frac{\lambda}{\mu_0} \nabla \cdot \vec{A} \right) = \vec{j} \ \dots \dots (6a)$$

with:

$$\vec{B} = \vec{\nabla} \times \vec{A} \ \dots \dots (6b)$$

The uniqueness of the magnetic potential vector is ensured by the fact that Eq. (6a) uses the Coulomb gauging. The second term on the left hand side of the equation is added as a penalty function[15,16] term in an ad-hoc manner in order to enforce the zero divergence of the magnetic field. The value for penalty factor λ must be chosen as small as possible, but large enough to quickly "push" the linear system towards the divergence free solution. In fact the numerical solution

to-hydrodynamic multiphase approach to simulate the flow, the temperature field, and the electrodynamics. The commercial software ANSYS-Fluent has been used for the flow and the thermal fields, the electromagnetic field was solved with a self-written code based on finite volume. The interfaces between the three different phases (metal, slag, gas) are tracked with a Volume of Fluid (VOF) method.[11,12] A single set of momentum equations is shared by the fluids, and the volume fraction of each fluid in each computational cell is tracked throughout the domain. According to the local value of the volume fraction f, appropriate properties and variables are assigned to each control volume within the domain. In a two phase system the properties appearing in the momentum equation are determined by the presence of the component phase in each control volume. The calculation domain contains a total of 145 000 cells. The time step is controlled by turbulence and the dynamic of the metal/slag interface through a chosen maximum courant number of 0.1. The detailed mathematical expressions of the boundary conditions used in the 2D simulations are presented in

fails to converge if the penalty factor is set to zero. Having tested the range [0,1] we noticed that the number of iterations to obtain satisfactory level of convergence decreases with an increase of λ. However, it was also noticed by some authors[16] that the accuracy of the solution decreases with an increase in the penalty factor. Therefore, when choosing the penalty factor considerations should be simultaneously given to convergence and solution accuracy. In the present 5 Hz problem, good convergence was obtained with a value of only 0.1.

Once the electric and magnetic field is solved, the time and space dependant Lorentz force acting on both slag and steel is obtained by:

$$\vec{F}_L = \vec{j} \times \vec{B} \quad \text{...................................} (7)$$

The electric current and the induced magnetic field are fully coupled with the phase distribution.

3.2. Heat Transfer and Electrode Melting

The energy equation is solved in the entire domain:

$$\frac{Dh}{Dt} = \nabla(k\nabla T) + Q(t) \quad \text{.........................} (8)$$

With $h = \rho(C_p T + \Delta H f_s)$ being the enthalpy, $Q(t)$ the Joule heating source and f_s a fictitious solid fraction defined by $f_s = \dfrac{T_L - T}{T_L - T_S}$. The Joule heating is taken as a source term in the energy equation:

$$Q(t) = \frac{j^2}{\sigma} \quad \text{...................................} (9)$$

where σ is the electric conductivity.

At the top boundaries a temperature of 300 K is assumed. The bottom boundary is set as outlet. In order to save computation time, the mould is not included directly in the calculation domain. At the air level, the melt pool level and the ingot level a combined convection-radiation heat transfer is considered. Corresponding values for the heat transfer coefficient, H, the mould temperature, T_e, and the emissivity of the mould surface, ε_r, are given in Table 2. In the present analysis the formation of the thin solid slag skin is not simulated. Between the liquid slag and the mould a thin solidified slag layer forms, it is commonly known as "slag skin". Thus the slag liquidus temperature is used as boundary condition whenever the slag phase is in contact of the mould. At the ingot level a good contact characterised by a heat transfer coefficient of $H = 1\,500$ W/(m²K) is assumed for the first 2 centimetres under the slag/pool interface. Under this level the heat transfer is assumed to be significantly reduced (Table 2). Material properties of steel and slag are listed in Table 1.

The electrode is physically assumed to melt at liquidus T_L temperature of the alloy (1 750 K). To solve numerically the problem of latent heat release at the solid/liquid interface, a fictitious solidus temperature was set $T_S = 1\,725$ K under the liquidus temperature. This numerical approach allows the latent heat to be released at least within 2 to 3 volume elements to avoid the occurrence of numerical errors. The solidification and the melting of the slag around the electrode is modelled in the same manner.

3.3. Flow Field and Lorentz Force

The incompressible Navier-Stokes equations for the liquid velocity $\vec{U}$ is solved. In between the liquidus and the fictitious solidus, a drag is applied to force the fluid velocity to become equal to the electrode descend speed:

$$\vec{F}_S = -(10^7 + 10^9 f_s)(\vec{U} - \vec{u}_e) \quad \text{................} (10)$$

In Eq. (10) the coefficient $(10^7 + 10^9 f_s)$ is chosen to be a linear function of the solid fraction.

The momentum equation includes both the drag and the Lorentz force,

$$\frac{D\rho\vec{U}}{Dt} = -\nabla p + \nabla(\mu\nabla\vec{U}) + H(1 - f_s) \cdot$$
$$\vec{F}_L + H(T_L - T) \cdot \vec{F}_S + \rho\vec{g}\beta(T - T_{ref}) \quad \text{..........}(11)$$

where H is the Heaviside step function, $H(x) = 0$ for $x < 0$ and $H(x) = 1$ for $x \geq 0$ and $T_{ref} = 1\,650°C$ for both slag and steel.

We have applied the above mentioned model to an ESR process in which the electrode temperature at the top boundary of the electrode is given and set constant. By assuming a constant electric current intensity, I_0, and a constant electrode descend speed, u_e, we tried to find a stable the electrode tip shape.

4. Energy Balance Analysis of Electrode by One Dimensional Model

Equation (3) with boundary conditions, Eqs. (4a) and (4b), is numerically solved for a $L_0 = 1$ m long electrode, initially at room temperature (300 K). Calculations were performed for 3 different electrode descend speeds, $u_e = 0.35$ mm/s, 0.14 mm/s, 0.08 mm/s. This range of speed is the one at which the ESR process is usually operating. In **Fig. 2** the variation of the heat flux from the melting interface into the electrode q is reported as function of the dimensionless remelting time t/t_0, where $t_0 = L_0/u_e$. The profile of q diverges at vicinity of $t = 0$. To achieve a finite melting rate an infinite heat flux must be provided to the electrode. Then q decreases, but stays at very high level during the first 5% of the remelting time. After this initial regime, the required heat flux decreases smoothly during the 80 to 90 % of the remelting time. This stage can be qualified as "steady melting state". To keep the melting rate constant, the last 5–10% of the remelting time requires much lower heat flux than during the steady state.

In the beginning of the process the building of the temperature gradient requires a very high heat input. Theoretically, at $t = 0$ achieving a non-zero melting rate requires an infinite heat input. This means that the desired melting rate cannot be achieved immediately in practically operation from the beginning, but should be progressively increased. At the end of the remelting, the temperature of the top extremity of the electrode is very close to the liquidus temperature, this is why only a small heat flux q is necessary.

During the steady state the amplitude of change of q is function of the electrode descend speed. A higher descend speed means smaller heating time for the electrode. The slower increase of the electrode temperature at the top position promotes quickly the occurrence of a steady heat bal-
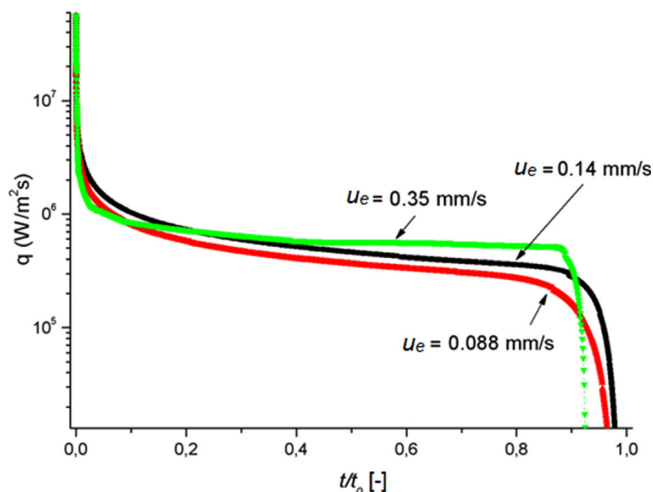
Fig. 2. Heat flux diffusing from the melting interface into the electrode, $q = -k \left. \dfrac{\partial T}{\partial x} \right|_{x=s(t)}$, versus the dimensionless melting time, t/t_0, for three different electrode descend rates. (Online version in color.)
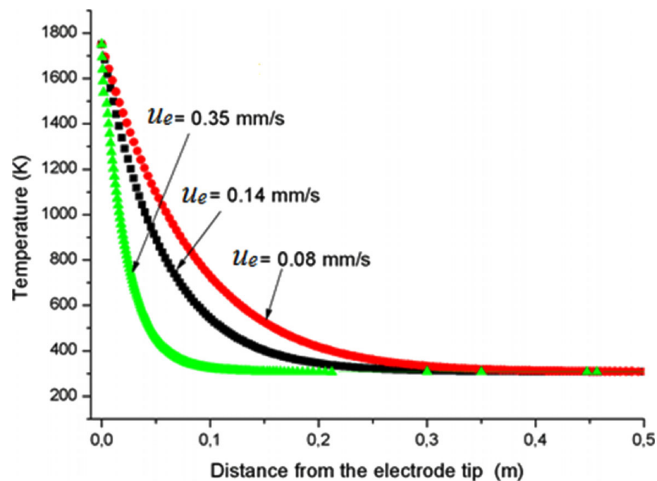
ance at the electrode tip. This is why the lower variations of q are achieved with higher descend speeds. During steady-state, the heat flux entering the electrode is equal to the sensitive heat necessary to bring the metal from the room temperature to the melting temperature

$$q(t,u) = \bar{Q} = u_e \int_{300K}^{T_{interface}} \rho C_p \, dT. \quad \text{................ (12)}$$

The time necessary to build the steady-state thermal boundary layer can be defined as the time at which q reaches 105% of $\bar{Q}$. For $u_e = 0.35$ mm/s we got $t = 142$ s which corresponds to a remelting length of 5 cm. For $u_e = 0.14$ mm/s we got $t = 1\,214$ s which corresponds to a remelting length of 17 cm and for $u_e = 0.35$ mm/s we got $t = 3\,125$ s which corresponds to a remelting length of 25 cm. These calculated results are the smallest theoretical times and distances over which a steady-state can be achieved. It assumes that the tip temperature reaches immediately the melting temperature. In practice especially during electrode change, the electrode preheating operation, which lasts for several hours, brings the electrode tip temperature from room temperature to about 700–900 K. It is only after this preheating process that the electrode is put in contact with the liquid slag.

In **Fig. 3** thermal boundary layers during the "steady-state plateau" for the three electrode descend speeds are shown. Here the thermal boundary layer thickness is defined as the distance from the electrode tip at which the temperature is 99% of the room temperature. The thickness of the steady-state thermal boundary layer varies strongly with the electrode descend speed. The smaller u_e the longer is the thermal boundary layer. Simulations targeting the melting rate are only valid by including a part of the electrode length longer than the thickness of the thermal boundary layer.

The electric current densities for small experimental electrodes such as those studied by Mitchell,[6] Mendryvowski[7] and Tacke[8] were of about 10^6 A/m^2. The resulting Joule heating generated in electrode ($j^2/\sigma \sim 10^6$–10^7 W/m^3) is then

Fig. 3. Thermal boundary layers during the "steady-state plateau" for three electrode descend rates. (Online version in color.)

Table 3. Geometry and process parameters.

Quantity	Value
Current intensity, frequency	4 000 A, 5 Hz
Melting rate	2 kg/min
Electrode descent rate u_e	0.366 mm/s
Mold thickness	3 cm
Slag height	140 mm
Electrode diameter ($2 \times R_e$)	130 mm
Ingot diameter ($2 \times R_m$)	200 mm
Initial electrode immersion depth	23 mm

as strong as the heat diffused into the electrode q (Fig. 2). Thus the Joule heat generation should not be neglected if the electrode temperature gradient is of interest. For industrial scale electrodes, the electric current density being lower ($\sim 10^4$–10^5 A/m^2), the Joule heating within the electrode is rather negligible ($j^2/\sigma \sim 10^4$ W/m^2).

5. ESR Process Simulation by Two Dimensional Model

In order to further explore the effect of the thermal state on the shape of the electrode we have applied the 2D axis-symmetrical magneto-hydrodynamic multiphase approach to a small ESR with the process parameters specified in **Table 3**. As boundary condition we have assumed that the electrode temperature at the top boundary is equal to room temperature. A large number of simulations were performed by varying the initial immersion depth of the electrode. Most of the results were found to be unstable. In some cases the electrode tip melting rate accelerated until the electrode tip finally quitted the liquid slag. In other cases the electrode melting rate was too weak to avoid an electric shortcut with the metallic pool. The origin of the instability is the coupling between the electrode immersion depth and the power generated by Joule heating. To picture the instability, let us consider a situation defined by a steady electrode tip shape and steady immersion depth resulting from the equilibrium of Eq. (4b). If at some time the heat provided by the slag is slightly higher, the melting of the electrode will decrease the

immersion depth. The increasing of electrode/pool distance results in a higher Joule heating generated in the slag. The slag temperature increases, which in turn increases the heat provided to the electrode and further shift the position of the electrode tip upward. Similarly, if the heat provided by the electrode is slightly lowered, the electrode immersion depth will decrease the power generated. The decrease of the slag

temperature, will lead to a downward instability motion where the electrode tip could finally touch the liquid metal pool. Without a numerical control of the electrode position it is not possible to avoid or stop this instability.

However, among all the simulations one configuration was found to be stable (**Figs. 4–8**). For this configuration, Fig. 4 shows the liquid and the other phase regions after the steady electrode and liquid pool shape is reached. The electrode tip shape is conical on the extremity and approximately flat at the centre of the electrode. It seems that this particular shape is less sensitive to the previously described instability; however the reason for that is not yet clear. The distribution
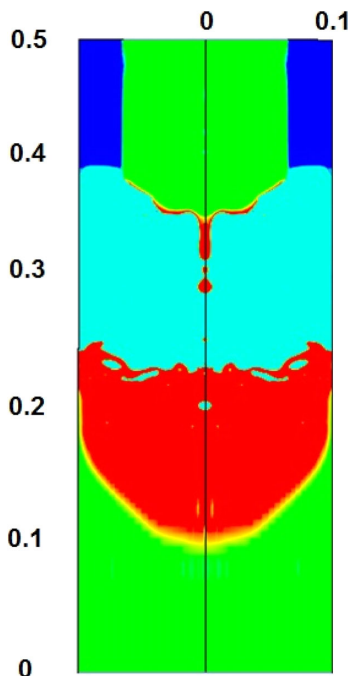

Fig. 4. Calculated phase distribution scaled in metres for the process parameters as specified in Table 3. (Red: liquid steel, Green: solid steel, Dark blue: air, light blue: liquid slag). (Online version in color.)
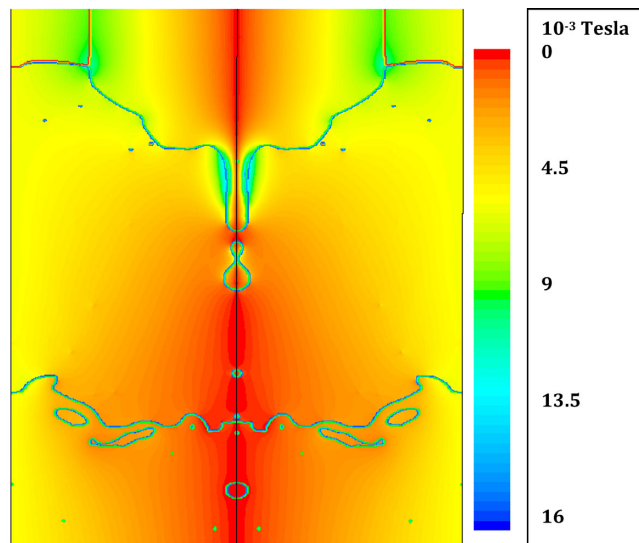

Fig. 6. Calculated distribution of the self-magnetic field for the process parameters as specified in Table 3. The width of the domain is 0.2 m. (Online version in color.)
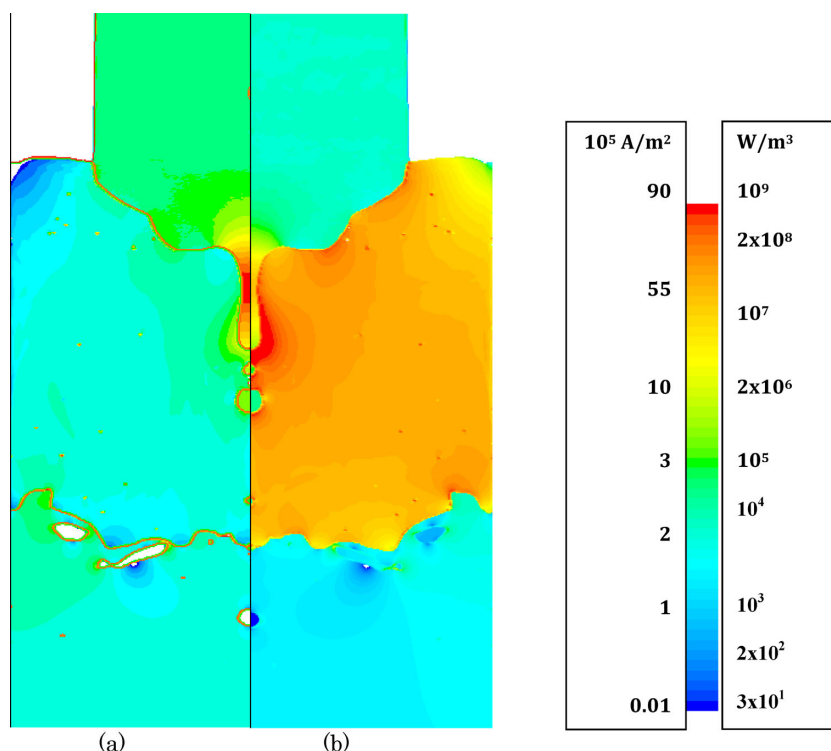

Fig. 5. Calculated distribution of the electric current density j (a) and joule heating source Q (b) for the process parameters as specified in Table 3. The width of the domain is 0.2 m. (Online version in color.)

of the electric current density (Fig. 5(a)) is controlled by the shape of the electrode, the presence of droplets as well as by the shape of the slag/pool interface. The maximum electric current density is extremely high (10^9 A/m^2). It is reached within the liquid metal faucet during a relatively short time (~0.1 s). Such current densities induce so strong electromagnetic pinch forces which break the liquid metal faucet into smaller droplets. The total power generated by the system can be obtained by calculating the integral of Eq. (9) over the entire calculation domain. In the present case, it fluctuates with the dripping but it is 240 kW in average. The maximum power generated follows the distribution of the electric current density, it is maximum near the surface of the electrode. Maximums are always reached at the electrode tip or at the faucet tip (Fig. 5(b)). High Joule heating is also generated in areas close to a concavely curved portion of the slag/pool interface. In fact, the combined action of the dripping and of the electromagnetic forces induces a strong interface motion. Some slag droplet penetrates the liquid pool.

When droplet formation is not considered the highest magnitude of the self-magnetic field is reached at the electrode/air surface. In the present case, the focussing of the electric current due to the presence of the liquid metal faucet generates area of high magnetic field intensity especially on the surface of the liquid metal faucet and droplets. As shown in Fig. 6, maximum (~0.015 Tesla) is reached which is two times higher than the one reached at the electrode surface (0.008 Tesla). Since the electrode surface is located outside the slag, these areas of high magnetic field intensity located in the slag bulk can have a higher impact on the hydrodynamic than the one developed near the electrode surface.

The resulting Lorentz force fluctuates as strongly as the electric current and the magnetic field during the melting.
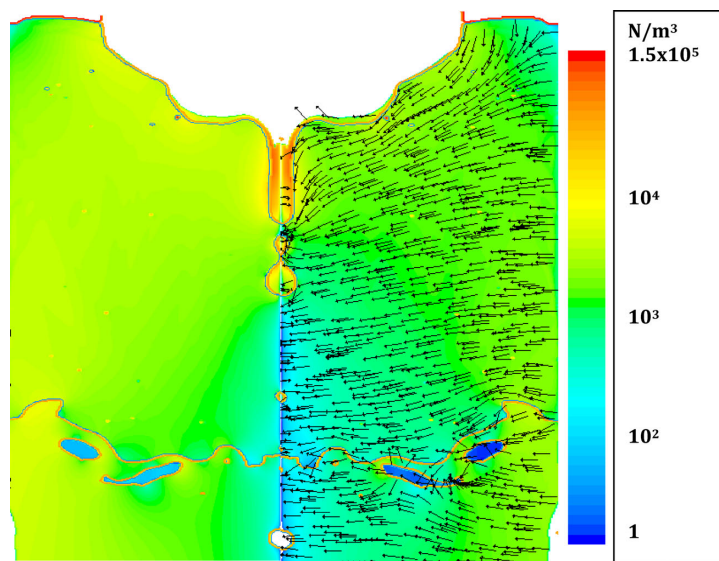

Fig. 7. Calculated magnitude and direction of Lorentz force for the process parameters as specified in Table 3. Colour scale refers to the magnitude and unified arrows to the direction of Lorentz force. The width of the domain is 0.2 m. (Online version in color.)
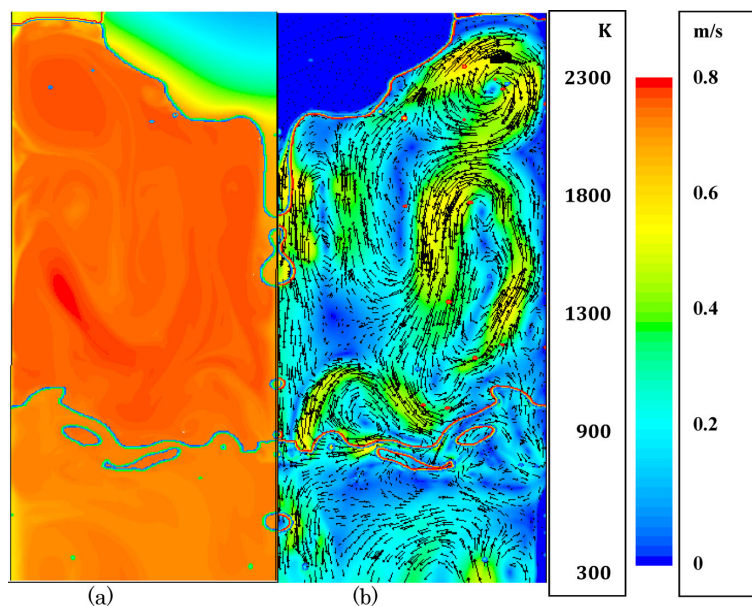

Fig. 8. Calculated temperature (a) and vlocity (b) fields for the process parameters as specified in Table 3. The width of the domain is 0.2 m. (Online version in color.)

Depending on the direction of the electric current, this force can be directed in all direction, even in the upward direction as it can be seen in Fig. 7. However most of the Lorentz force vectors are oriented in the inward radial direction. The hydrodynamic is controlled by the competition between the Lorentz force, the thermal buoyancy, and the mass transfer due to the falling droplets. Near the electrode the Lorentz force drives the slag flow in the downward direction (Fig. 7). However, it can be seen that in these areas the liquid is mostly flowing upward (Fig. 8(b)). The reason is the thermal buoyancy generated by the strong thermal gradient between the hot slag and the "cold" electrode surface (Fig. 8(a)). This convection is even more promoted by the inclined surface of the electrode. The electromagnetic force dominates in the centre where the electric current is highly concentrated. Near the slag/metal interface the thermal gradient is in the stable configuration (Fig. 8(a)), the only forces in action are the electromagnetic forces and the forces resulting from the droplet impacts. The maximum slag flow velocities are in the range of 0.3–0.5 m/s. However falling droplet could reach velocities up to 0.7 m/s. During the melting large droplets were emitted at a frequency of about 3 Hz. Due to the droplet formation and to the slag/metal interface movement the electric current lines are continuously changing. The average bulk slag temperature is about 2 100 K, the level of turbulence is high enough to limit the temperatures differences to about 200 K (Fig. 8(a)).

An extensive study of the stability of the present configuration results is beyond the scope of this paper. It could be conducted by dynamically adjusting the electrode immersion depth while keeping a constant electrode descend velocity.

6. Conclusions

A numerical analysis of the energy balance of the electrode has been performed to explore the different thermal states of electrode during remelting process. In order to melt an electrode with a constant melting rate, a time varying heat flux must exists between the slag and the electrode. The required heat flux follows three regimes. The first regime is characterised by extremely strong heat fluxes. Then a steady state regime starts with a smooth decrease in heat flux. During the melting the average temperature of the electrode is continuously increasing. At the last regime, the electrode is warm enough to be melted with only small heat input.

Additionally, a numerical model assuming 2D axisymmetric flow and no mould current was used to simulate a real ESR process. The results have shown that the melting of an electrode with constant electrode descend velocity is inherently an unstable process. One stable or metastable configuration was found and presented in detail in this paper. The stable electrode tip is approximately flat at the centre and conical in the peripheral regions. During the melting the electromagnetic variables such as the electric current, the magnetic field, and the Lorentz forces are highly fluctuating. Instabilities resulting from the coupling between the electrode melting (shape and movement) and the electromagnetic field need further investigations. Furthermore as in a real ESR process, the stability can be achieved in the simulation results only by including a numerical control of the electrode immersion depth in the slag.

REFERENCES

1) G. K. Bath: Proc. 1st Int. Symp. of Electroslag consumable Electrode Remelting and Casting Tech., Mellon Inst. Pittsburgh, PA, (1967), 1.
2) A. Mitchell and S. Joshi: *Metall. Trans.*, **4** (1973), 631.
3) A. Jardy, D. Ablitzer and J. Wadier: *Metall. Trans. B*, **22B** (1991), 111.
4) A. Kharicha, M. Wu and A. Ludwig: EPD Congress 2011, ed. by S. N. Monteiro, D. E. Verhulst, P. N. Anyalebechi and J. A. Pomykala, John Wiley & Sons, Inc., Hoboken, NJ, USA, (2011).
5) A. Kharicha, M. Wu, A. Ludwig, M. Ramprecht and H. Holzgruber: CFD Modeling and Simulation in Materials Processing, ed. by L. Nastac, L. Zhang, B. G. Thomas, A. Sabau, N. El-Kaddah, A. C. Powell and H. Combeau, John Wiley & Sons, Inc., Hoboken, NJ, USA, (2012), 139.
6) A. Mitchell, S. Joshi and J. Cameron: *Metall. Trans.*, **2** (1971), 561.
7) J. Mendrykowski, J. J. Poveromo, J. Szekely and A. Mitchell: *Metall. Trans.*, **3** (1972), 1761.
8) K. H. Tacke and K. Schwerdtfeger: *Arch. Eisenhüttenwes.*, **52** (1981), 137.
9) T. F. Zien: *AIAA J.*, **16** (1978), 1287.
10) J. J. Beaman, R. L. Williamson and D. K. Melgaard: Proc. of Int. Symp. LMPC, ed. by A. Mitchell and J. Van Den Avyle, American Vacuum Society, USA, (2001), 161.
11) A. Kharicha, W. Schützenhöfer, A. Ludwig , G. Reiter and M. Wu: *Steel Res. Int.*, **79** (2008), 632.
12) A. Kharicha, W. Schützenhöfer, A. Ludwig and G. Reiter: *Int. J. Cast Met. Res.*, **22** (2009), 155.
13) A. Kharicha, A. Ludwig and M. Wu: *Mater. Sci. Eng. A*, **413** (2005), 129.
14) A. Kharicha, W. Schützenhöfer, A. Ludwig and G. Reiter: *Mater. Sci. Forum*, **649** (2010), 229.
15) O. Biro and K. Preis: *IEEE Trans. Magn.*, **25** (1989), 3145.
16) H. Y. Lin, L. M. Tu, L. Udpa and Y. S. Sun: *IEEE Trans. Magn.*, **35** (1999), 1354.